Oxidation of Sputtered Thin Films of Molybdenum Alloys at Ambient Conditions

A. List*,**, C. Mitterer*, G. Mori**, J. Winkler***, N. Reinfried*** and W. Knabl***

* Department of Physical Metallurgy and Materials Testing, Montanuniversität, Leoben, Austria

** Department of General, Analytical and Physical Chemistry, Montanuniversität, Leoben, Austria

*** PLANSEE Metall GmbH, Reutte, Austria

Abstract

Room temperature oxidation of Mo in the presence of humidity may deteriorate its properties in thin film applications like thin film transistor liquid crystal displays or photovoltaic cells. To improve their oxidation resistance, Mo films of 200 nm thickness, alloyed with the elements Ti, Cr, Ni, Nb, Ta, or W, respectively, have been grown by magnetron co-sputtering from Mo mosaic targets with the respective alloying element inserts. All coatings show single-phase solid solutions. The respective alloying content is determined by the number of target inserts, their respective sputter yield and the scattering probability during transport from the target to the substrate, and could be confirmed by SRIM calculations. Electrical resistivity values are comparable to those of unalloyed Mo. Corrosion properties have been determined in 85 % humidity at 85°C by use of exposure tests in a climatic chamber. Potentiodynamic and electrochemical impedance spectroscopy were additionally done in 0.9 % NaCl aqueous solution at room temperature. Cr was identified as the alloying element resulting in the highest corrosion resistance due to formation of a passive layer.

Keywords

Molybenum films, alloying, sputtering, oxidation, corrosion

Introduction

Molybdenum thin films are widely used for photovoltaic cells and thin film transistor liquid crystal displays (TFT-LCD) due to their relatively low electrical resistance and easy chemical patterning. It has been frequently observed that their storage in moist air leads to superficial oxidation of Mo. Although its oxidation behavior has been intensively investigated at high temperatures [1], little has been reported about the oxidation of Mo in air at room temperature. For high-purity bulk Mo, the most decisive parameter for oxidation at a temperature of 40°C and relative humidity of 98 % seems to be the pre-treatment and the surface roughness, where oxide layers with a thickness of 15-20 nm are formed after 168 hours of exposure [2]. These intensively colored oxide films cause optical irritation and reduce the electrical conductivity, thus limiting the application of Mo films in TFT-LCDs.

Consequently, several studies have been done to improve the low-temperature oxidation and corrosion properties of Mo films. Park et al. report on spontaneous passivation of sputtered Mo-Ti alloy films in 12 M HCl, where corrosion rates lower than those of the pure components have been observed for the range between 20 and 60 at.-% Ti [3]. Also Tomachuk et al. mention a superior corrosion behavior of Mo-Ti films compared to Mo-Nb [4].

The aim of this study was to evaluate the effect of low contents of the alloying elements Ti, Cr, Ni, Nb, Ta, or W, respectively, in sputter deposited Mo films on their oxidation and corrosion resistance. In pursuit of this goal, relations between thin film synthesis conditions, resulting film structure and composition have been established. Electrical, oxidation and corrosion properties have been determined by a four-point method, by exposure in a climatic test chamber and by potentiodynamic polarization experiments and electrochemical impedance spectroscopy in 0.9 % NaCl aqueous solution.

Experimental details

Mo thin films have been grown in a laboratory-scale unbalanced magnetron sputtering system described in detail in ref. [5]. A Mo target with a purity of ≥ 99.97 wt.-% and 152 mm diameter, mounted to an unbalanced Gencoa PP150 magnetron, has been used. For depositing alloyed films, 24 inserts of 5 mm diameter of the elements Ti, Cr, Ni, Nb, Ta, or W, respectively, have been placed in blind holes evenly distributed over the erosion track of the Mo “mosaic” target. The target-to-substrate distance was 7.5 cm. As substrates, alkaline earth boro-aluminosilicate glass sheets for display technologies (Corning EAGLE2000TM AMLCD) of dimension 50.8 × 50.8 × 0.7 mm have been used, which have been cleaned before deposition using a commercial detergent from Borer Chemistry for glass cleaning. For thin film deposition, the sputtering power was 1 kW and the Ar pressure 0.3 Pa. The substrate temperature was set to 120°C, and a bias voltage of -50 V was applied to the substrates. After pre-sputtering of the target for 10 min and substrate ion etching for 5 min at -1250 V, films with thicknesses of ~2.5 µm (deposition time, 20 min) and ~200 nm (deposition time, 100 sec) were grown. The thicker films have been used for determining the chemical composition and the growth rate, while structural investigations as well as characterization of electrical, corrosion and oxidation properties has been done on the thinner films.

The film thickness was characterized using scanning electron microscopy (SEM, Zeiss EVO-50) on fractured cross-sections and 3D optical profilometry (Wyko NT1000) on the steps of partly masked and thus uncoated substrate areas. The chemical composition was determined using energy-dispersive X-ray spectroscopy (EDS, Oxford Instruments INCA) attached to the SEM. The efficiency of sputtering at the target was simulated using the SRIM code (The Stopping and Range of Ions in Matter, version 2008.05 [6]). For estimation of thermalization behavior of energetic species sputtered from the target, the scattering characteristics during the transport phase from the target to the substrate was characterized by the energy transfer coefficient ε [7]

$$\varepsilon = \frac{4 \cdot m_1 \cdot m_2}{(m_1 + m_2)^2} \quad (1)$$

There, m_1 is the mass of atoms sputtered from the target and m_2 is the mass of Ar. X-ray diffraction (XRD) was done using a Bruker-AXS D8 Advance diffractometer with Cu Kα radiation in Bragg-Brentano geometry. The macro-strain in the films was calculated via the XRD peak shift, while the micro-strain was estimated via peak broadening using a Pseudo-Voigt function. The film resistivity was measured by a four-point probe method using a MDC Multiheight Probe.

The oxidation and corrosion properties of the films were evaluated by three different tests. Exposure tests were done in a climatic test chamber at 85 % humidity at 85°C for 168 h (1 week). Potentiodynamic and electrochemical impedance spectroscopy were additionally done in 0.9 % NaCl aqueous solution at room temperature. As reference electrode, a saturated calomel electrode (SCE) at a potential of 241 mV_{SHE} (standard hydrogen electrode) was used. The starting potential was 100 mV lower than the open

circuit potential (OCP). The scan rate was 600 mV/h and the reverse potential was 200 mV_{SCE}. Electrochemical impedance spectroscopy was done by application of a tube cell onto the specimens surface. Measurements were done at OCP after 0, 4 and 24 h of immersion with an alternating voltage of ±10 mV in a frequency range between 1 mHz and 500 kHz. After exposure in the climatic test chamber, the corroded film surfaces were characterized using a Jobin-Yvon LabRam confocal Raman spectrometer (Nd–YAG laser; wavelength, 532.2 nm; power, 10 mW).

Results and discussion

The film growth rate was calculated from film thickness measurements and the corresponding deposition time to ~2.1 nm/sec, and was not significantly affected by the alloying elements. The alloying content as determined by EDS was in the range between 3.2 and 5.2 at.-% (see Table I). The observed differences between the used alloying elements can be explained by their different sputter yields and scattering characteristics. SRIM calculations of the sputter yield gave a low value for Ti, which means that these inserts are less efficiently sputtered than Mo. Thus, for the Mo-Ti system the flux of sputtered species leaving the mosaic target shows a lower alloying element concentration as compared to the target composition in the erosion track. In addition, Ti shows a high energy transfer coefficient, due to its atomic mass comparable to Ar, indicating quick thermalization of sputtered Ti atoms, thus explaining the relatively low alloying content of the film (see Table I). On the other hand, Cr with the highest sputter yield observed as well as Ta and W with also relatively high yields, high energies per sputtered atom and low energy transfer coefficients show significantly higher alloying concentrations. The concentration observed for Ni is relatively low, which might be due to its ferromagnetic nature providing a short-circuit for the magnetic field lines of the magnetron. The reasons for the high Nb alloying content are presently unclear, and it has to be mentioned that the Mo and Nb peaks overlap in EDS, giving rise to a higher uncertainty in determining the Nb content. It has also to be noted that we did not consider the likely different condensation behavior of the individual atoms at the substrate, due to lacking literature data.

Table I: Summary of investigated Mo alloy film systems with their respective alloying content, atomic mass, sputter yield, energy per sputtered atom and energy transfer coefficient.

Alloying element	Alloying content [at.-%]	Atomic mass	Sputter yield	Energy per sputtered atom [eV]	Energy transfer coefficient
Mo	100	96	1.11	34.3	0.83
Ti	3.4 ± 0.2	48	0.64	28.1	0.99
Cr	4.7 ± 0.7	52	1.43	18.3	0.98
Ni	3.2 ± 0.1	59	1.97	21.0	0.96
Nb	5.2 ± 1	93	0.77	40.9	0.84
Ta	3.8 ± 0.5	181	0.96	29.7	0.59
W	4.0 ± 0.1	184	1.04	31.8	0.59

All coatings deposited show well-defined peaks of the Mo phase in the XRD patterns, indicating the formation of a single-phase Mo-based solid solution for all alloying elements. This is attributed to the film growth conditions in magnetron sputtering, which are far away from thermodynamic equilibrium [8] and allow formation of supersaturated solid solutions. No significant effect of the alloying elements on the grain size of the Mo-based solid solution was observed (see Table II).

Nevertheless, a more detailed analysis of the XRD peaks indicated slight changes, as summarized in Table II. For Cr, Ni and W, representing smaller or similar-sized atoms as Mo, macro-strains which are lower than those of unalloyed Mo films are observed, whereas for the larger Nb and Ta atoms higher macro-strains have been obtained. Similar arguments hold for the micro-strain induced by the elements Cr, Nb and Ta. While these simple interpretations are well suited to explain the strain generated by alloying of Mo films with most of the elements used in this study, Ti does not seem to follow this trend. However, it has to be admitted that in explaining solid solutions not only the effect of lattice distortion has to be taken into account, but also the change in elastic properties and the chemical interaction between the individual atoms.

Table II also shows the electrical resistivity of the films as determined by the four-point probe. The resistivity of the unalloyed Mo film agrees well to literature data [9,10,11]. While alloying with Ti, Cr, Nb, Ta, and W does not affect the values significantly, the addition of Ni results in a three times higher resistivity.

Table II: Summary of investigated alloying systems with the atomic radius of the respective alloying element, the film grain size, the diffraction angle 2 θ of the (110) XRD peak, the determined lattice spacing, the macro-strain calculated from the XRD peak shift of the (110) peak, the micro-strain calculated from the broadening of the (110) peak using a Pseudo-Voigt fitting function, and the determined electrical resistivity of the films.

Alloy system	Atomic radius [pm]	Grain size [nm]	2 $\theta_{(110)}$ [°]	Lattice spacing [nm]	Macro-strain	Micro-strain	Electrical resistivity [μΩcm]
Mo	136	42	40.41	0.2230	0.00223	0.00279	11
Mo-Ti	144	37	40.48	0.2226	0.00057	0.00233	15
Mo-Cr	125	45	40.53	0.2224	-0.00061	0.00263	14
Mo-Ni	125	43	40.44	0.2229	0.00152	0.00293	33
Mo-Nb	142	37	40.33	0.2234	0.00413	0.00295	14
Mo-Ta	143	48	40.37	0.2232	0.00318	0.00288	14
Mo-W	137	54	40.49	0.2226	0.00033	0.00261	12

The cathodic and the anodic electrochemical behavior of Mo and Mo alloy films, as measured in a 0.9 % NaCl aqeous solution against a saturated calomel electrode, is shown in Fig. 1. It can clearly be seen that there are only small differences in the corrosion potentials and the corrosion current density of the individual films. The corrosion current density was measured to 0.13 μA/cm^2 for the Mo samples alloyed with Cr and Ni, 0.17 μA/cm^2 for the Mo-Nb film and 0.24 μA/cm^2 for those films alloyed with Ti, Ta and W. All these values are lower compared to the current density measured for Mo, i.e. 0.26 μA/cm^2. However, it has to be mentioned that the differences between the alloy systems for both, the corrosion potential and the corrosion current density, are relatively small and close to the statistical measurement error. To illustrate this, additional measurements were done for three film samples of the Mo-Cr system, being coated in the same deposition run. There, a corrosion potential of -270 ± 40 mV_{SCE} and a corrosion current density of 0.13 ± 0.03 μA/cm^2 was obtained. This means that the scattering of data for the corrosion potential is almost in the same order of magnitude as the differences measured (see Fig. 1). Nevertheless, from the corrosion current density one can conclude that Cr and Ni are most efficient in improving the corrosion rate, whereas Ti, Ta and especially W do not affect the corrosion current density significantly compared to the unalloyed Mo film.

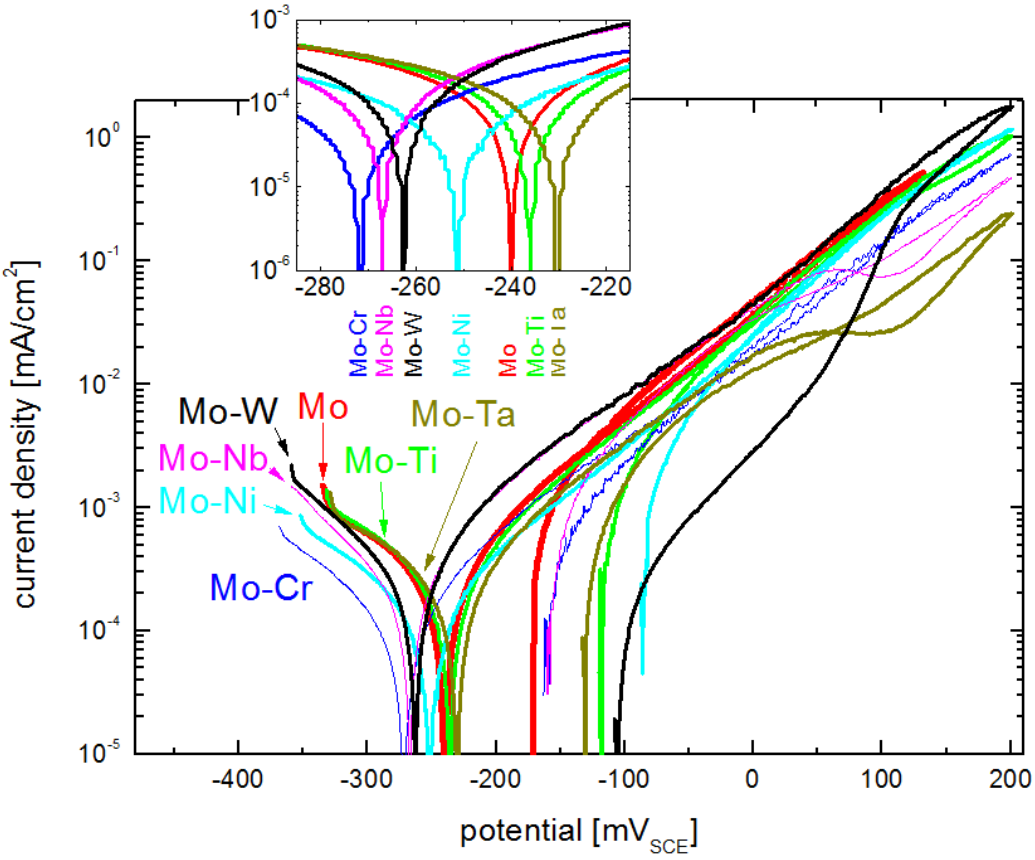

Fig. 1: Cathodic and anodic polarization curves of the Mo alloy thin film systems investigated.

To determine the polarization resistance of the samples at the corrosion potential without disturbing the system significantly, electrochemical impedance spectroscopy in a 0.9 % NaCl aqueous solution was used. The polarization resistance was calculated from the Nyquist plots shown in Fig. 2 after 24 h of immersion. Already the Nyquist plots indicate that alloying the Mo films with Ti, Ni, Nb, Ta, and W only results in small changes, and likewise also the polarization resistance is only slightly affected (see Fig. 2). However, adding Cr results in a dramatic change of the Nyquist plot and an increase of the polarization resistance from values around 20 to 116 kΩ. The lowest polarization resistance (equal to the highest corrosion rate) was obtained for Mo and Mo-W films.

Fig. 3 shows the specific mass gain as obtained after 168 h exposure of the coated samples in a climatic test chamber at 85°C and 85 % relative humidity. It has to be noted that the measured mass changes are in the range of 10 to 320 µg, where the lower values are close to the resolution limit of the precision balance used. Nevertheless, it can be seen from Fig. 3 that essentially no specific mass gain was obtained for those Mo films alloyed with Ti and Ta, whereas the highest values have been observed for the unalloyed Mo film and for alloying with Ni and W. This corresponds also to the visual appearance of the film surfaces after exposure, where intense blue colorations are seen for Mo, Mo-Ni and Mo-W, while the other films show yellowish to brownish colors.

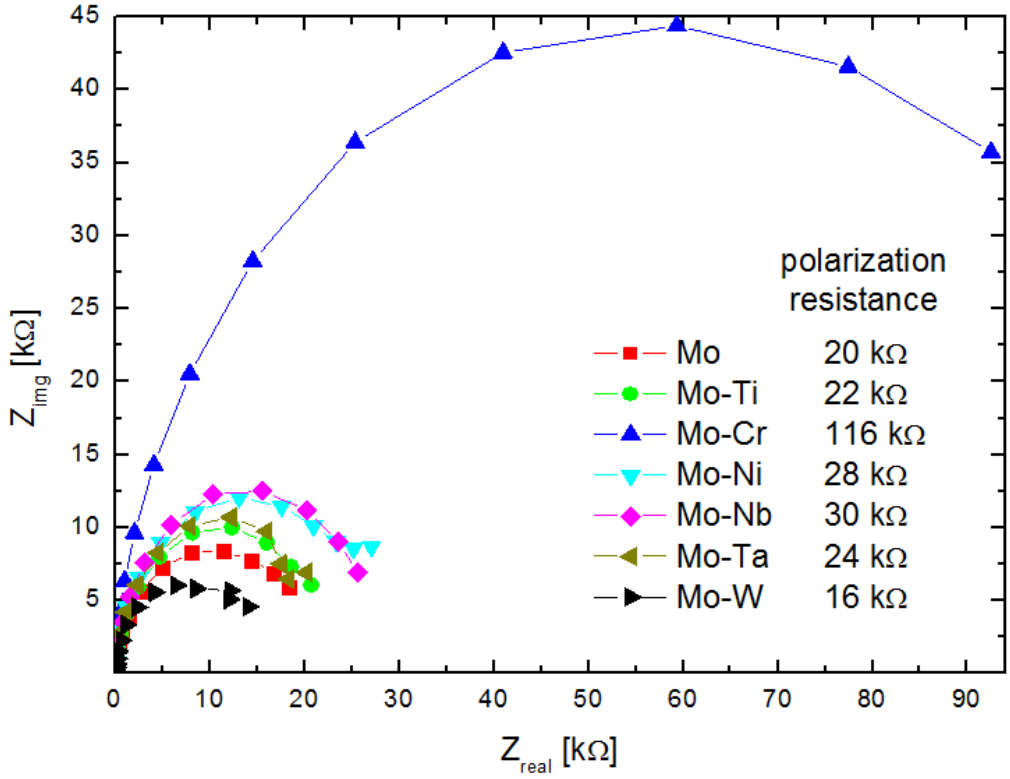

Fig. 2: Nyquist-diagram of Mo alloy thin films in 0.9 % NaCl aqeous solution (room temperature, open circuit potential, ±10 mV, 1 mHz – 500 kHz) after 24 h of exposure to the test solution. The respective polarization resistance is also given.

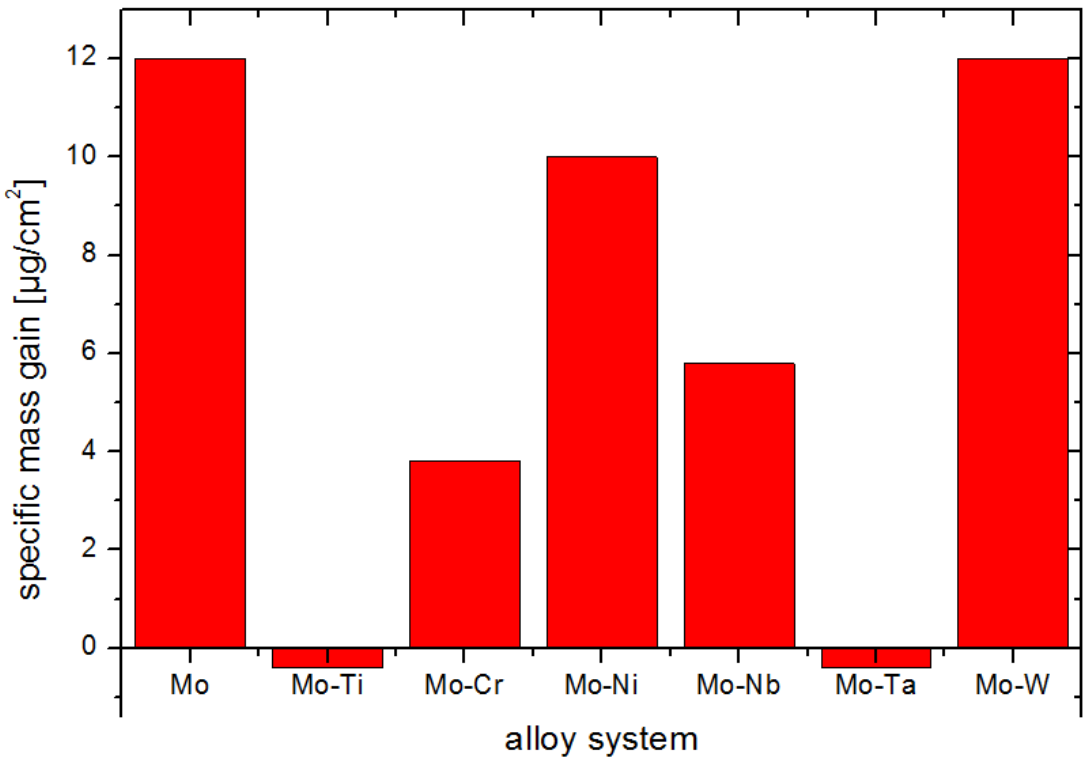

Fig. 3: Specific mass gain of the Mo alloy thin film systems investigated as determined by corrosion tests at 85°C and 85 % relative humidity.

The oxide films formed during exposure in the climatic test chamber are too thin to be detected by XRD and in SEM cross-sections [2]. To obtain more information about their nature, Raman spectroscopy investigations have been done on the oxidized film surfaces. Usually, metals are not Raman active, whereas oxides often show intense Raman bands [12]. This is in good agreement with Fig. 4, where no significant intensity of Raman peaks is observed for the as-deposited Mo film surface. The surfaces after exposure to the climatic test chamber show peaks indicative for formation of MoO_2 and MoO_3 [13,14], as confirmed by the Raman spectra of MoO_2 and MoO_3 powders also shown in Fig. 4. It has to be noted that the peaks found on the surfaces of the oxidzed films are less sharp and broader, as compared to the powder standards. This might be due to the low thickness and high structural disorder of the oxide layers formed during low-temperature oxidation.

The low intensity observed for the Mo-Ta film correlates well with the low specific mass gain shown in Fig. 3. While the positions of the Raman peaks do not show significant differences for the unalloyed film and for alloying with Ti, Ni, Nb, and W, the Mo-Cr film shows – in addition to the peaks originating from MoO_2 and MoO_3 – a pronounced Raman peak at ~880 cm^{-1}, which is related to the formation of chromium oxides [15,16]. It can thus be concluded that these chromium oxides show a passivating nature, explaining the excellent performance of Mo-Cr films in electrochemical impedance spectroscopy (see Fig. 2) and during exposure in the climatic test chamber (see Fig. 3). It is surprising that already such low Cr contents of 4.7 at.-% (Table I, corresponding to 2.6 wt.-% Cr) in the Mo film are sufficiently high to form a Cr-rich oxide layer at the surface. In stainless steels, this threshold Cr value is 12 wt.-%. The reason for this is not clear yet, however, investigations on Cr-containing cemented carbides proved that also Cr-concentrations in the binder alloy of only 5 wt.-% are sufficient to improve the corrosion resistance significantly [15]. These binders also contain high amounts of W that acts chemically similar like Mo.

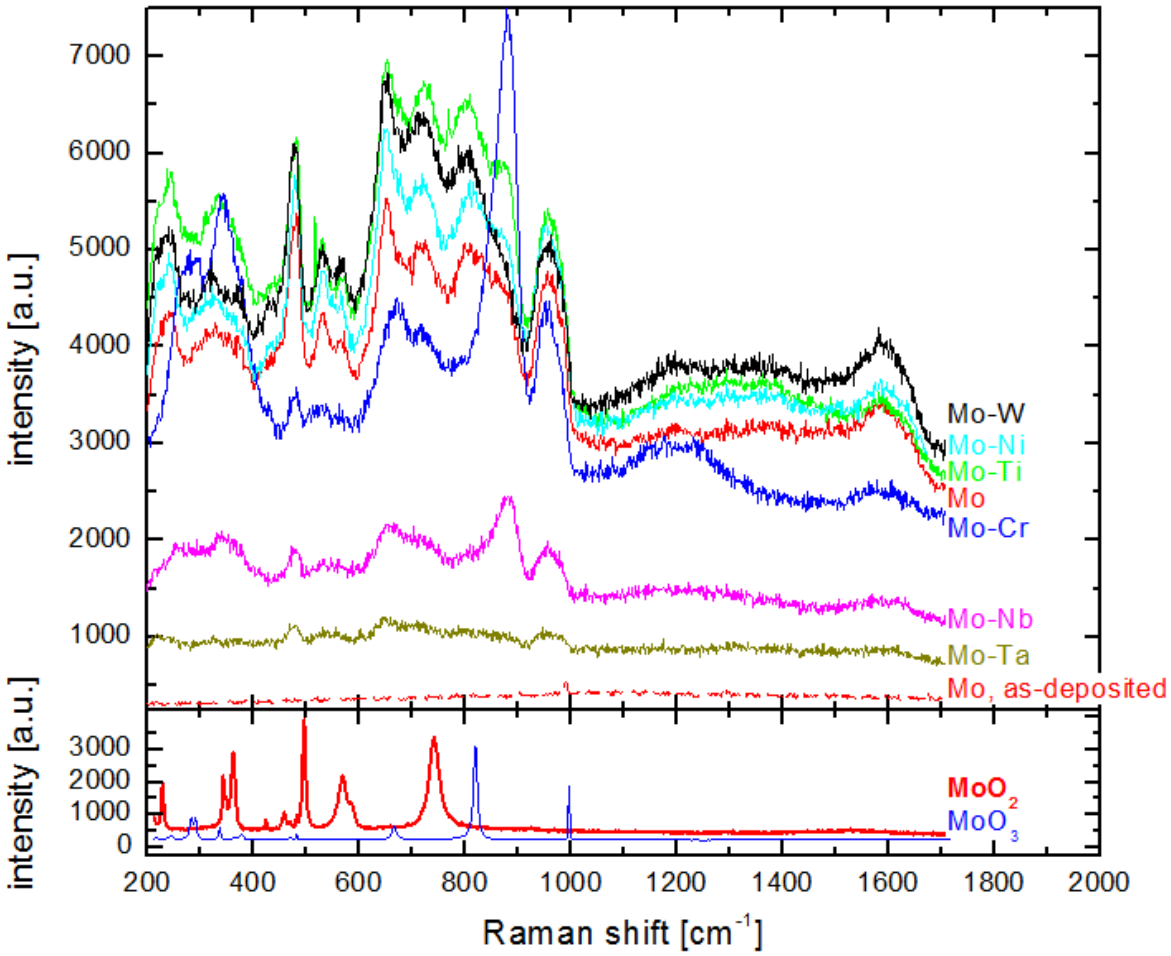

Fig. 4: Raman spectra of the as-deposited Mo film and the Mo alloy systems oxidized at 85°C and 85 % relative humidity. The Raman spectra of MoO_2 and MoO_3 powders are given for comparison.

Conclusions

Molybdenum thin films, alloyed with Ti, Cr, Ni, Nb, Ta, or W, respectively, have been synthesized on glass substrates by magnetron sputtering from mosaic targets. In all cases, the content of the alloying elements was below 5.2 at.-% and single-phase Mo-based solid solutions are formed. The observed differences in corrosion and oxidation behavior are relatively small, nevertheless, some general tendencies can be drawn from the combination of tests performed. Alloying with Cr results in the lowest corrosion current density in electrochemical polarization experiments, the highest polarization resistance in electrochemical impedance spectroscopy and the Mo-Cr sample is within the top three ones in the exposure test in the climatic test chamber. These excellent corrosion properties are related to the change of oxide film structure from pure Mo oxide towards a Cr-enriched oxide film. While Ti, Ni, Nb, and Ta show a corrosion and oxidation performance better than the unalloyed Mo films, alloying by W does not show a benefical effect. This is most probably due to the similar chemical behavior and oxide structure of Mo and W.

Acknowledgement

A part of this work has been supported by the Austrian Research Promotion Agency (FFG) under the framework of the Research Studio Austria Surface Engineering.

References

1. N. Birks, G.H. Meier and F.S. Pettit, *Introduction of the High-Temperature Oxidation of Metals*, 2nd Ed., Cambridge University Press, Cambridge, (2006)
2. M. Gritsch, C. Brunner, K. Piplits, H. Hutter, P. Wilhartitz, A. Schintlmeister and H.P. Martinz, *Fresenius J. Anal. Chem.* **365** [1-3], 188-194, (1999)
3. P.Y. Park, E. Akiyama, H. Habazaki, A. Kawashima, K. Asami and K. Hashimoto, *Corros. Sci.* **38** [10], 1649-1667, (1996)
4. C.R. Tomachuk, D.B. Mitton, J. Springer, T. Monetta and F. Bellucci, *Mater. Corros.* 57 [5], 394-399, (2006)
5. P. Losbichler and C. Mitterer, *Surf. Coat. Technol.* **97** [1-3], 567-573, (1997)
6. http://www.srim.org
7. M. Ohring, *Materials Science of Thin Films*, p. 164, Academic Press, San Diego (2002)
8. I. Petrov, P.B. Barna, L. Hultman and J. E. Greene, *J. Vac. Sci. Technol. A* **21** [5], 5117-5128, (2003)
9. K.Y. Ahn, J.M. E. Harper, P.M. Fryer, B. Davari, L. Krusin-Elbaum and J. Karasinski, *Proceedings 3rd Workshop on Tungsten and other Refractory Metals for VLSI Applications*, Materials Research Society, Warrandale, pp. 317-326, (1988)
10. F. Martin, P. Muralt and M.-A. Dubois, *J. Vac. Sci. Technol. A* **24** [4], 946-952, (2006)
11. F. Klabunde, M. Löhmann, J. Blasinq and T. Drüsedau, *J. Appl. Phys.* **80** [11], 6266-6273, (1966)
12. W.H. Weber, *Raman Scattering in Materials Science*, Springer, Berlin, (2000)
13. M. Dieterle, G. Weinberg and G. Mestl, *Phys. Chem. Chem.* Phys. **4** [5], 812-821, (2002)
14. M. Dieterle and G. Mestl, *Phys. Chem. Chem. Phys.* **4** [5], 822-826, (2002)

15. D. Stanoi, G. Socol, C. Grigorescu, F. Guinneton, O. Monnereau, L. Tortet, T. Zhangd and I.N. Mihailescu, *Mater. Sci. Engin. B* **118**, 74-78, (2005)

16. B.M. Weckhuysen and I.E. Wachs, *J. Phys. Chem. B* **101**, 2793-2796, (1997)

17. S. Sutthiruangwong, G. Mori and R. Koesters, *Int. J. Refract. Met. Hard Mater.* **23**, 129-136, (2005)